Toward Omnidirectional Light Absorption by Plasmonic Effect for High-Efficiency Flexible Nonvacuum $Cu(In,Ga)Se_2$ Thin Film Solar Cells

Shih-Chen Chen,[‡] Yi-Ju Chen,[§] Wei Ting Chen,[∥] Yu-Ting Yen,[§] Tsung Sheng Kao,[†] Tsung-Yeh Chuang,[⊥] Yu-Kuang Liao,[‡] Kaung-Hsiung Wu,[‡] Atsushi Yabushita,[‡] Tung-Po Hsieh,[⊥] Martin D. B. Charlton,[#] Din Ping Tsai,[∥,⊗] Hao-Chung Kuo,[†,*] and Yu-Lun Chueh[§,*]

[†]Department of Photonics and Institute of Electro-Optical Engineering and [‡]Department of Electrophysics, National Chiao-Tung University, Hsinchu 30010, Taiwan, [§]Department of Materials Science and Engineering, National Tsing Hua University, Hsinchu 30013, Taiwan, [∥]Department of Physics, National Taiwan University, Taipei 10617, Taiwan, [⊥]Compound Semiconductor Solar Cell Department, Next Generation Solar Cell Division, Green Energy and Environment Research Laboratories, Industrial Technology Research Institute, Hsinchu, Taiwan, [#]School of Electronics and Computer Science, University of Southampton, Highfield, Southampton SO17 1BJ, United Kingdom, and [⊗]Research Center for Applied Sciences, Academia Sinica, Taipei, Taiwan

ABSTRACT We have successfully demonstrated a great advantage of plasmonic Au nanoparticles for efficient enhancement of $Cu(In,Ga)Se_2$(CIGS) flexible photovoltaic devices. The incorporation of Au NPs can eliminate obstacles in the way of developing ink-printing CIGS flexible thin film photovoltaics (TFPV), such as poor absorption at wavelengths in the high intensity region of solar spectrum, and that occurs significantly at large incident angle of solar irradiation. The enhancement of external quantum efficiency and photocurrent have been systematically analyzed *via* the calculated electromagnetic field distribution. Finally, the major benefits of the localized surface plasmon resonances (LSPR) in visible wavelength have been investigated by ultrabroadband pump−probe spectroscopy, providing a solid evidence on the strong absorption and reduction of surface recombination that increases electron−hole generation and improves the carrier transportation in the vicinity of *pn*-juction.

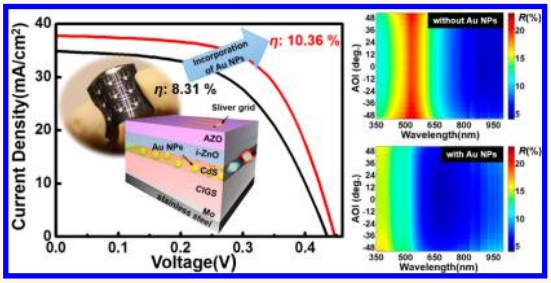

KEYWORDS: solar Cell · $Cu(In,Ga)Se_2$ · omnidirectional light absorption · plasmonic effect · nanoparticles · flexible

The energy crisis that has arisen from the decreasing reserve of combustible fuel is one of great impacts to the world that we are currently facing. Greenhouse effects resulting from the side products of combustible fuel significantly accelerate hazardous climate change. Therefore, finding environmentally friendly and sustainable energy to meet energy demands and reduce climate change is crucial. Energy harvesting by photovoltaic (PV) methods has been regarded as a favorable candidate among renewable energies because the amount of solar radiation reaching to the earth's surface in one hour can sufficiently provide one year's worth of humanity's energy demand. For materials as PV, silicon-based materials, including single and poly crystalline structures, which are the leading materials, have been extensively studied. However, drawbacks such as indirect bandgap and poor light absorption could result in unsatisfied conversion efficiency for Si-based solar cells.[1]

Alternatively, $Cu(In,Ga)Se_2$ (CIGS) is the most promising material owing to its excellent light-trapping ability, broadband light absorption, and environmentally friendly manufacturing processes. The chalcopyrite compound materials have abundant advantages, including high environmental tolerance,[2] long-term stability,[3,4] and remarkable absorption characteristics.[5] The highest efficiency of 20.9% on $CuIn_{1-x}Ga_xSe_2$ (CIGS) thin-film solar cells has been achieved, which is the highest recorded efficiency among all thin-film photovoltaics (TFPVs).[6] Various deposition methods for CIGS thin films have been developed, including vacuum processes (coevaporation,[7] sputtering,[8] and pulsed laser deposition[9]) and nonvacuum processes

* Address correspondence to hckuo@faculty.nctu.edu.tw, ylchueh@mx.nthu.edu.tw.

Received for review June 18, 2014 and accepted August 5, 2014.

Published online August 05, 2014
10.1021/nn503320m

(ink-printing,[10] and electrochemical deposition[11]). Among these fabrication processes, the ink-printing method is an attractive approach for development of flexible CIGS TFPV devices because of mass production and low cost nonvacuum device fabrication. To further promote the CIGS TFPV light absorption ability throughout the full solar spectrum range, extensive efforts have been devoted, including bandgap management through different doping concentrations[12] and various postprocessing procedures, to placing or creating nanostructures on the CIGS absorber layer,[13] while some unwanted defects may be generated, hindering further practical applications.[14]

The plasmonic effect, for which the surface charges of mental nanostructures are triggered by electromagnetic waves, can be collectively oscillated as set of resonances known as surface plasmons.[15] The plasmons appearing in a localized area at the interface between two materials are known as localized surface plasmon resonances (LSPR), which are created in a limited volume of metal nanostructures.[16] Metal conduction electrons in high conduction metals, particularly gold (Au), silver (Ag), and copper (Cu), can coherently trigger the LSPR as a collective. By adjustment of particle diameter, shape, and surrounding materials, a large fraction of oscillator strength of electrons into the proper spectral ranges can be controllably tuned.[17−22] The optical cross sections for absorption and scattering can be enhanced due to the massive engaged metallic conduction electrons, such that the projected geometrical area of a plasmonic particle can even span over an substantial spectral range.[20,23] Thus, manipulation of the plasmon resonances into the required spectral range is a principal issue for photovoltaic applications.[24−26] In this regard, we demonstrate the plasmonic effect based on gold nanoparticles, which are embedded between the *pn*-junction interface of CIGS TFPV, to increase the electron-hole generation and thus enhance the photocurrent. With the properly designed layer structure, for which the interface of CdS/CIGS has been found to be the suitable choice for distribution of Au NPs, the conversion efficiency of the plasmonic CIGS flexible thin-film solar cells with embedded Au nanoparticles can be promoted, especially at large incidence angles. Analyses of the enhancement of external quantum efficiency and photocurrent by the plasmonic Au nanoparticles (NPs) were investigated in detail. To further investigate the enhancement mechanisms, the electromagnetic field distribution of plasmon modes at different spectral ranges has been calculated *via* finite element (FEM) simulation. Finally, the ultrafast carrier dynamics of plasmonic CIGS thin film have been delineated by the ultrabroadband femtosecond pump−probe spectroscopy.

RESULTS AND DISCUSSION

Figure 1a shows the absorption spectrum (green color) and the corresponding photo image of a CIGS *pn*-junction fabricated by ink-printing process on a stainless steel substrate. Obviously, in the range of 500−600 nm from the absorbance spectra of the CIGS *pn*-junction, poor light absorption can be observed, which may result from the undesirable coverage and the poor quality of the CdS layer on the rough CIGS surface.[27] It is a critical problem because this range belongs to wavelength regions of high intensity in the solar spectrum. As a result, great enhancement of light-to-electricity efficiency can be expected if this drawback can be tackled. For such a purpose, we introduced the Au NPs with a diameter of ~10 nm, whose plasmonic resonance is located at a wavelength

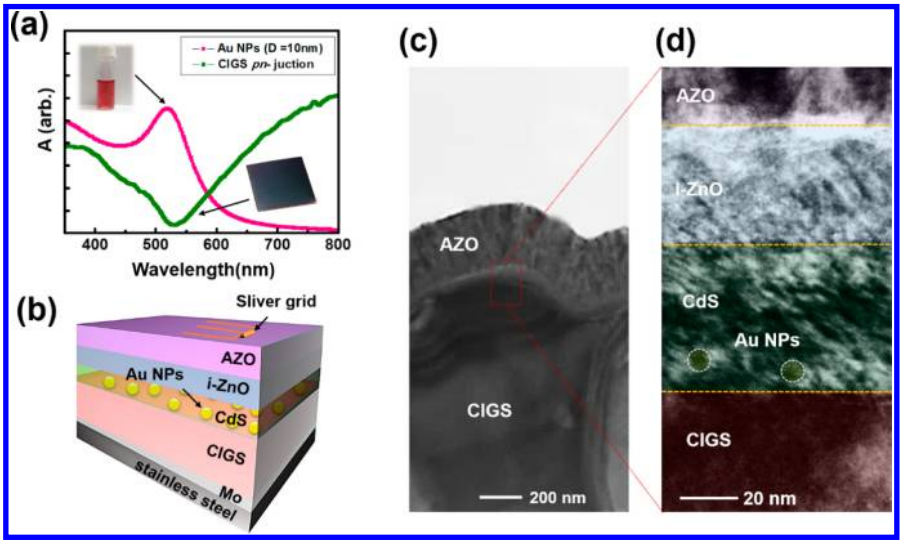

Figure 1. (a) Absorption spectra and photo images of CdS/CISG *pn*-junction of ink-printing CIGS TFPV and gold nanoparticles solution. (b) Schematic layer structure of plasmonic CIGS TFPV. (c) TEM image of the plasmonic CIGS TFPV. (d) High-resolution TEM image of a selected area at the interface between CdS and CIGS.

of ~530 nm as shown in the red curve in Figure 1a. The inset also shows the corresponding photo image of the Au NPs solution. For the fabrication of the CIGS solar cell, Mo back contact deposited on flexible stainless steel foil was prepared as the substrate. A precursor layer was prepared *via* the nonvacuum nanoparticle method and coated on the substrate by an ink-printing process. After the postselenization and the KCN washing process, the *p*-type CIGS absorber layer was accomplished. Then, plasmonic Au nanoparticles with a diameter of 10 nm were sprayed on the CIGS layer *via* air brush with low nitrogen gas flow. Through the chemical bath deposition, a cadmium sulfide (CdS) thin film was deposited on the Au nanoparticles layer where plasmonic nanoparticles were located at the *pn*-junction interface of CIGS/CdS. The buffer layer and transparent conductive oxides, i-ZnO and Al:ZnO(AZO), were capped on the *pn*-junction. Finally, the silver grid was coated by a printing process. The ultimate device structure is schematically shown in Figure 1b. To confirm the existence of the Au NPs between CIGS *pn*-junction, a TEM image was conducted as shown in Figure 1c. Figure 1d shows the corresponding high-resolution TEM image taken from rectangular area in Figure 1c. Obviously, the Au NPs (~10 nm) embedded between CdS and CIGS can be observed and are marked by the white dash circles in Figure 1d.

The effect of Au NPs on light absorption on the CdS/CIGS *pn*-junction was examined before the device was accomplished. The absorption enhancement factor defined by ratio of absorption intensity with and without Au NPs ($A_{\text{with Au NPs}}/A_{\text{without Au NPs}}$) in the CdS/CIGS *pn*-junction are shown in Figure 2a at different incident light wavelengths. The absorption enhancement factor >1 can be obviously observed, indicating the enhanced light absorption in the CdS/CIGS *pn*-junction, which is attributed to the superposition of various plasmonic modes of different arrays of Au NPs by comparing the absorption spectrum with Au NPs (Figure 1a) while the red-shifted behavior due to different surrounding materials can be found as well.[24] Note that the peak enhancement factor arisen from plasmonic resonance of Au NPs is broad due to the random distribution of Au NPs.[24] On the other hand, a small decrease at shorter wavelengths (<450 nm) and longer wavelengths (>800 nm) are most likely attributed to the energy dissipation[28,29] and the backward scattering[30,31] by Au NPs, respectively. The latter one can be compensated and is beneficial after deposition of i-ZnO and AZO layers on the junction owing to the increase of absorption through the Fabry–Perot interferences.[32,33] To shed light on enhanced absorption by the plasmonic effect for possible application on flexible TFPV, the measurements of optical properties on the fabricated plasmonic CIGS thin-film samples were conducted by using angle-resolved reflectance spectrometer. The corresponding

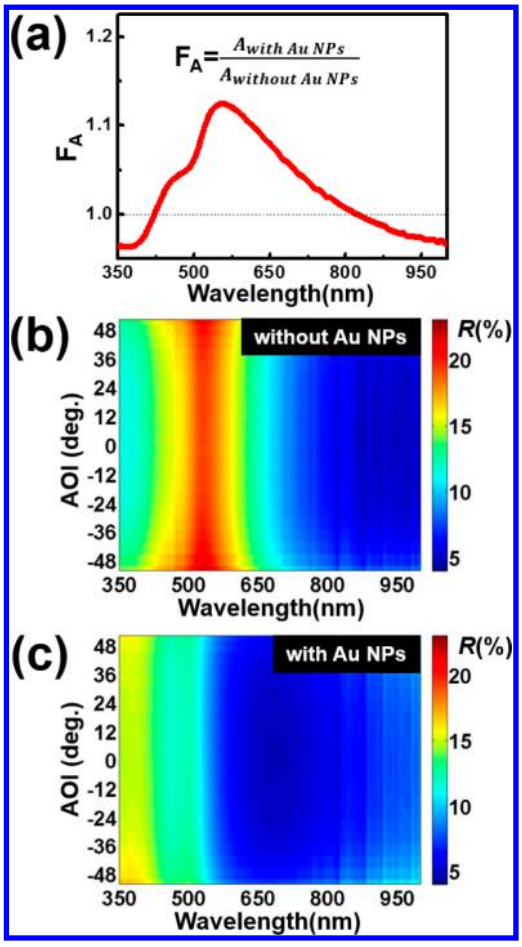

Figure 2. (a) Absorption enhancement factor of the plasmonic CIGS TFPV. Angle-resolved reflectance spectra of the (b) conventional and (c) plasmonic CIGS TFPVs. A strong elimination of light reflectance can be found in the spectra of the plasmonic CIGS TFPV in the visible range of 500–700 nm.

reflectance spectra of the conventional and plasmonic CIGS thin-film solar cells obtained at different angle of incidence (AOI) are shown in parts b and c of Figure 2, respectively. Obviously, a strong elimination of light reflectance in the visible range of 500–700 nm can be found in the CIGS photovoltaic device with Au NPs (plasmonic CIGS thin-film solar cell) compared with the CIGS photovoltaic device without Au NPs (conventional CIGS thin-film solar cell). The significant absorption region following the high optical intensity region in solar spectrum reflects the great feasibility of the photocurrent enhancement. Thus, with the strong plasmonic resonance of Au nanoparticles, one may improve the poor light absorption, which results from the undesirable coverage and poor quality of the CdS layer on the rough CIGS nanoparticle surface. On the other hand, the conventional CIGS exhibits higher reflectance at lager incident angles that give a restriction on the application of the flexible TFPV. Such high reflectance at large incident angles can be significantly suppressed after the incorporation of Au NPs, which enables integration of CIGS TFPV to infrastructures with various

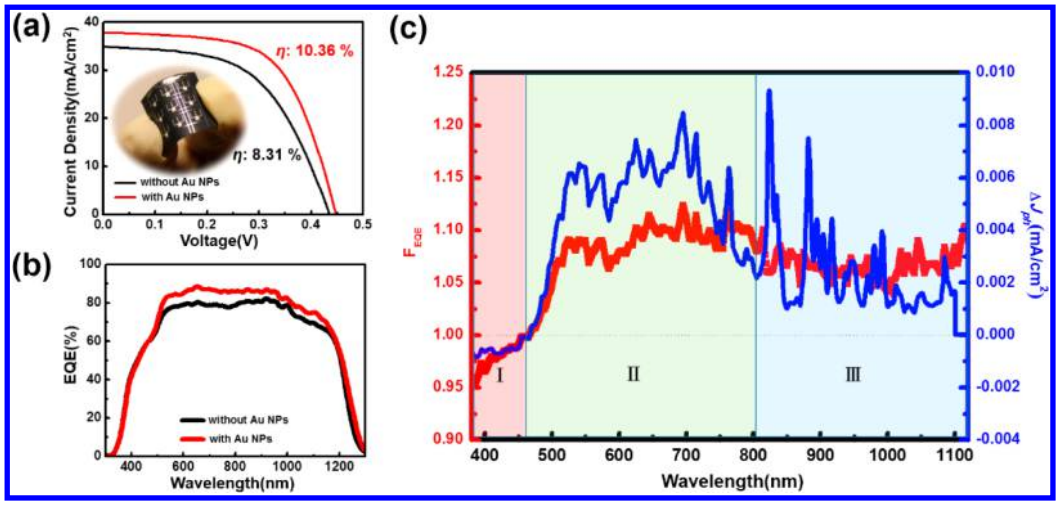

Figure 3. (a) Comparison of the *J*−*V* characteristics between conventional (black) and plasmonic (red) flexible CIGS TFPV. (b) Comparison of the EQE curve between conventional (black) and plasmonic (red) flexible CIGS TFPV. (c) Enhancement factor of the EQE(red) and photocurrent ΔJ_{ph}(blue) of plasmonic CIGS TFPV.

geometrical conditions. In addition, we also demonstrated another layer structure design whose Au NPs were placed in the interface of the CdS/i-ZnO layer rather than in the interface of the CdS/CIGS *pn*-junction (Figure S1a, Supporting Information). The TEM and the corresponding high-resolution TEM images as shown in Figure S1b (Supporting Information) distinctly confirm the existence of Au NPs marked by white circles, at which the diameters of Au NPs with ~10 nm was found. The angle-resolved reflectance of Au NPs in the interface of the CdS/i-ZnO layer as shown in Figure S2 (Supporting Information) reveals that the reflectance can be decreased in the wavelengths between 500 and 600 nm due to surface plasma resonance of Au NPs but cannot be effectively decreased in omnidirectional directions as the best layer structure design.

In addition to the optical properties, the electric properties of the plasmonic CIGS thin film solar cell were also quantitatively characterized. The results with a comparison to the conventional CIGS photovoltaic device are shown in Figure 3a. The *J*−*V* characteristics show that the light-to-electricity efficiency can be enhanced from 8.31% to 10.36% with the incorporation of Au NPs to harvest more incident light energy at the plasmonic resonance regions. The corresponding Voc, Jsc, FF, and efficiency are listed in Table 1. The inset shows a photo image of a fabricated plasmonic CIGS flexible TFPV. It is worth noting that the strong near-field signal of the plasmonic modes not only enhanced the photocurrent by generating more electron−hole pairs but also improved the open-circuit voltage from 0.44 to 0.45 V with an enhanced filling factor from 54.77 to 61.25%. The improved Voc and FF may be related to significant reduction of surface recombination at the interface of the CdS/CIGS *pn*-junction and will be discussed later.[34,35] A comparison between the external quantum efficiency (EQE) spectra of conventional and plasmonic flexible CIGS photovoltaic devices are shown in Figure 3b. The EQE spectrum of the plasmonic CIGS device shows significant enhancement throughout wavelengths ranging from 500 to 1100 nm. In order to investigate the mechanism of the efficiency enhancement in the plasmonic CIGS photovoltaic device, enhancement factor of the EQE by ratio of $EQE_{with\ Au\ NPs}/EQE_{without\ Au\ NPs}$ and enhanced photocurrent $\Delta J_{ph} = J_{ph}$ (with Au NPs) $- J_{ph}$ (without Au NPs) were plotted by red and blue lines as the function of the light wavelengths as shown in Figure 3c. Obviously, the enhanced EQE of ~5−10% in a broadband range of 500−1100 nm can be confirmed, which is most likely attributed to the localized surface plasmon resonance (LSPR) of Au NPs embedded in the interface of the CdS/CIGS *pn*-junction.[32] In addition, the LSPR can trigger more electron−hole pairs, and thus, distinctly enhanced ΔJ_{ph} at wavelengths of 500−800 nm can be achieved for the plasmonic CIGS PV cell (blue curve in Figure 3c). However, as for the region of longer wavelengths (>800 nm), the enhanced EQE factor may result from the expected rescattering of incident light by Au nanoparticles. However, there are no significant enhancement in photocurrent due to the weaker intensity of solar spectrum in this region. Abrupt peaks in this region correspond to the spectrum of the light source. The poor performance at wavelength <450 nm as marked at the red region in Figure 3c is most likely attributed to energy dissipation and backward scattering of light by Au NPs, which is consistent with the absorption spectra in Figure 2a.

TABLE 1. Comparison of the *J*−*V* Characteristics between Conventional and Plasmonic Flexible CIGS Photovoltaic Devices

flexible CIGS TFPV	V_{oc} (V)	J_{sc}(mA/cm^2)	FF (%)	efficiency (%)
without Au NPs	0.44	34.84	54.77	8.31
with Au NPs	0.45	37.81	61.25	10.36

All of the PV characterizations discussed above were performed with normal incident light. However, the conversion of light into electric energy occurring at a wide range of incident light should be considered for practical PV applications. To investigate the enhancement of conversion efficiency at different angles of light irradiation, the angle-resolved $J-V$ characteristics measurements were conducted as shown in Figure 4a.

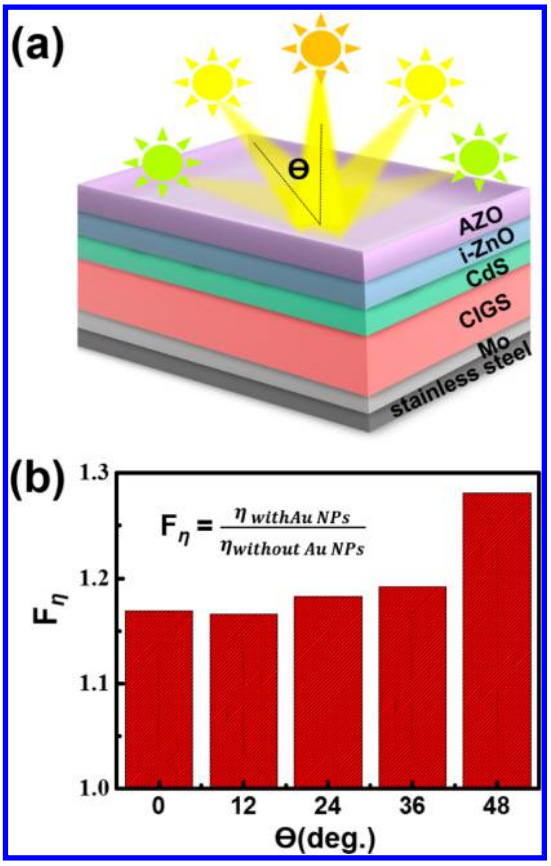

Figure 4. (a) Schematic of angle-resolved $J-V$ characteristics measurements. (b) Enhancement factor of conversion efficiency at different incident angles of light irradiation.

The average of acquired efficiency enhancement factors defined by the ratio of efficiency calculation with and without Au NPs in the interface of the CdS/CIGS *pn*-junction ($\eta_{\text{with Au NPs}}/\eta_{\text{without Au NPs}}$) are shown in Figure 4b at different irradiation angles from normal to 48° with respect to the surface of the device. Clearly, the conversion efficiency can be more significantly enhanced at a large operating angle (>40°) from the plasmonic CIGS photovoltaic devices due to the excellent omnidirectional absorption. The results demonstrate that the plasmonic CIGS TFPV are quite suitable for the practical applications of flexible TFPV.[36] In addition, the angle-resolved efficiency enhancement from $J-V$ measurements for another layer structure design (see Figure S1a,b, Supporting Information) was also measured (Figure S3, Supporting Information). Obviously, the plasmonic CIGS TFPV with Au NPs in the interface of the CdS/i-ZnO layers cannot maintain the similar angle-resoled $J-V$ characteristic, with which the enhanced factors of conversion efficiency were suppressed with the large angle of incident angles. The results are also agreement with the angle-resoled reflectance mapping at different incident angles that the enhanced absorption by Au NPs is not omnidirectional (Figure S2, Supporting Information). As a result, it can be concluded that the best location for placing Au NPs is in the interface of the CdS/CIGS *pn*-juction of the plasmonic CIGS TFPV.

Furthermore, a finite element method (FEM) was adopted to calculate the electromagnetic field distribution in order to elucidate the plasmonic modes, which enhance the performance of plasmonic CIGS TFPV.[37,38] Note that we found that the LSPR of Au NPs was excited with different field distributions in regions II and III indicated as the green and blue color regions from Figure 3c in parts a and b, respectively, of Figure 5. At region II (Figure 3c), as this LSPR mode was excited, there were very strong near-field regions in the vicinity of the gold particle, especially near the interface of the

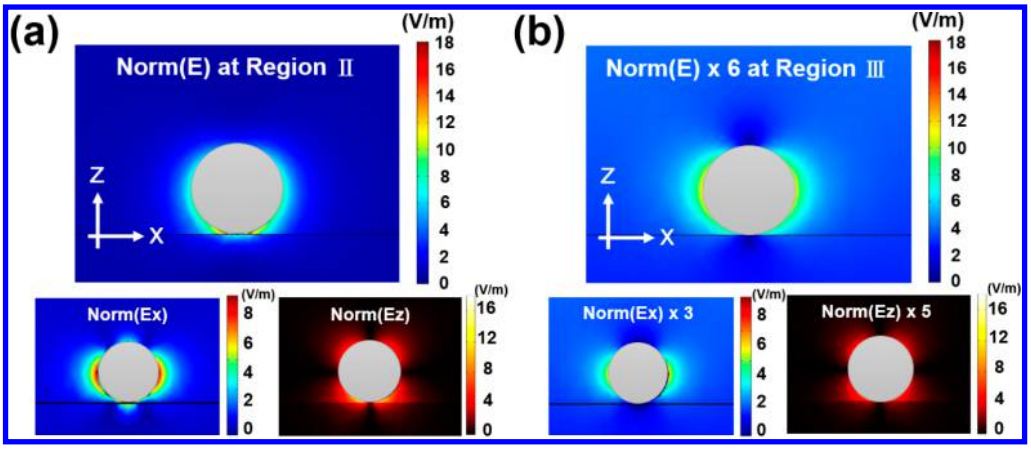

Figure 5. Distributions of electric fields for plasmon resonance at (a) region II and (b) region III calculated by finite element (FEM) method.

CdS/CISG *pn*-junction (Figure 5a), and the strong near-field region of the LSPR mode can penetrate into the CIGS absorber layer. This strong near-field region can be significantly enhanced by gap resonance, while there is a gap between Au NPs and the interface of *pn*-juction.[39] We also demonstrated the electromagnetic field distribution in Figure S4 (Supporting Information). Thus, a larger amount of incident light was concentrated and absorbed in this field, generating more photoexcited carriers (electron−hole pairs). There are more affected zones in the CIGS absorber layer by the tilted near-field region, which arise from the incident light at large angle. That explains the omnidirectional absorption behavior, resulting in a great enhancement in conversion efficiency at higher incident angle (Figure 4b). In addition, the strong field nearby the interface of the CdS/CIGS *pn*-junction can trigger an additional external force to enhance the carrier extraction, by which surface recombination of carriers can be significantly reduced, resulting in the improvement in electrical transport properties to enhance Voc and FF (Table 1), respectively.[32,34] However, in region III, the conventional field distribution of LSPR occurred (Figure 5b). The near-field profiles of the dipolar mode are distributed on the both sides of the gold nanoparticle, which mainly result in an increase of the scattering cross-section, triggering more rescattering activities. Such a phenomenon is beneficial to the utilization of incident light for a solar cell. Therefore, the enhanced photocurrent can be also acquired in the long wavelength region (blue region in Figure 3c).[25]

To further verify our speculation, we investigate the ultrafast carrier dynamics of plasmonic CIGS thin film by ultrabroadband pump−probe spectroscopy. Pump−probe spectroscopy has been commonly used for carrier recombination studies, particularly Shockley−Read−Hall (SRH) recombination.[40−42] Here, the samples were pumped and probed by an ultrabroadband femtosecond pulsed laser. The transient absorptivity changes ($\Delta A/A$) corresponded to the relaxation process of photoexcited carriers. Quantitatively, the higher intensity of ($\Delta A/A$) indicates a larger amount of excited carriers, while the longer relaxation time implies the less SRH recombination rate.[40−42] The corresponding ultrabroadband pump−probe spectra for the CIGS thin films without and with Au NPs are shown in parts a and b, respectively, of Figure 6. After the incorporation of Au NPs, we found more excited carrier at the wavelengths where LSPR occurs in region II, which is attributed to strong near-field region near the Au NPs. We have quantitatively confirmed the increase of excited carrier by using moment analysis as shown in Figure S5 (Supporting Information).[43] In addition, longer carrier relaxation time can also be observed in this region, which is ascribed to the strong field in the vicinity of the interface of the CdS/CISG *pn*-juction. The strong field improved the poor transportation of carriers at the interface by the effective reduction of surface recombination, which is consistent with the observations of the significant improvement in electrical transportation in *J*−*V* measurements when the Au NPs was incorporated. The demonstration of the LSPR in visible wavelength in flexible CIGS provides solid evidence of the strong absorption and reduction of surface recombination that increases electron−hole generation and improves the carrier transportation in the vicinity of the *pn*-juction.

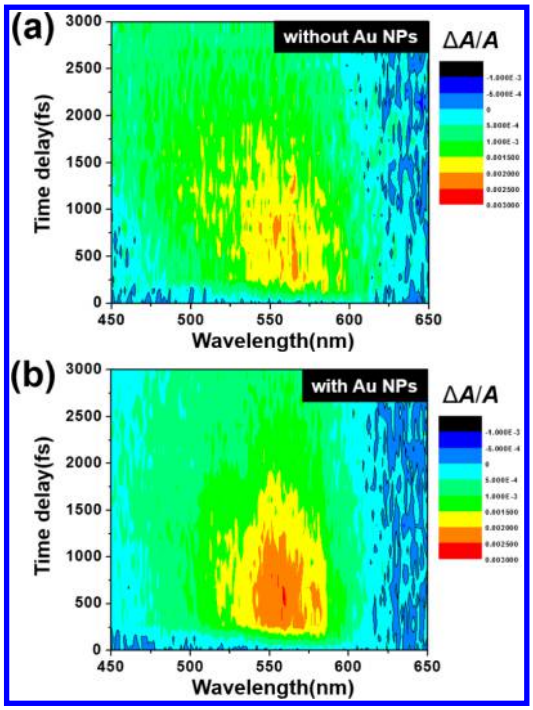

Figure 6. Ultrabroadband pump−probe spectra mapping images for the (a) conventional and (b) plasmonic CIGS TFPV at different wavelengths.

CONCLUSION

In this work, we have successfully demonstrated the great advantage of plasmonic Au nanoparticles for efficiency enhancement of CIGS flexible photovoltaic devices. The incorporation of Au NPs can eliminate obstacles in the way of developing ink-printing CIGS flexible TFPV, such as the poor absorption at wavelengths in the high intensity region of the solar spectrum, which occurs at a large incident angle of solar irradiation. The enhancement of external quantum efficiency and photocurrent have been systematically analyzed *via* the calculated distributions of electric field. Finally, the major benefits the LSPR at shorter wavelength have been investigated by ultrabroadband pump−probe spectroscopy, which gives solid evidence of the strong absorption and reduction of surface recombination that increases electron−hole generation and improves the carrier transportation

in the vicinity of *pn*-juction. These results suggest a promising method for rapidly improving the performance of CIGS flexible photovoltaic devices at low cost.

EXPERIMENTAL METHODS

Preparation CIGS Absorber Layer by Ink-Printing Process. The CIGS thin films were prepared by a nonvacuum nanoparticle synthesis method. The nanoingredients of copper oxide, indium oxide, and gallium oxide were dispersed in water-based solution by utilizing the agent. The solid content of the stable ink was about 20 g/100 mL. A scalpel was employed to coat the precursor film on the Mo/Cr/stainless steel substrate. Then, the precursor was reduced under H_2 atmosphere at 450 °C for 30 min. At the end, the precursor was annealed in H_2Se atmosphere at 400 °C for 30 min.

Characterizations. A UV−vis−NIR spectrophotometer (Hitachi U4100) with standard mirror optics and an integrating sphere was used to measure the absorptance of the CIGS *pn*-juction and Au NPs in the 350−800 nm range at normal incidence. The angle-resolved reflectance spectroscopic system used a custom-built 15 cm-radius integrating sphere with a motor-controlled rotational sample stage in the center, and a broadband 300 W xenon lamp was employed to carry out the angle-resolved mapping image. Then, the collected reflectance photons were resolved by a spectrometer (SPM-002-ET, Photon-control Inc.) to acquire the reflective spectrum with respect to different AOIs. The system was calibrated by the reflective spectrum of a NIST-standard, intrinsic Si at normal incidence.

In order to analyze the characterization of devices, *J*−*V* measurements were conducted, closely following the procedure described in international standard CEI IEC 60904-1. Both the CIGS solar cells and the reference cell were measured under a simulated Air Mass 1.5, Global (AM1.5G) illumination with a power of 1000 W/m^2. The temperature was actively maintained at 25 ± 1 °C during the measurements. Power conversion efficiency (PCE) measurements were performed for further characterization. The PCE measurement system consisted of a power supply (Newport 69920), a 1000 W Class A solar simulator (Newport 91192A) with a xenon lamp (Newport 6271A), an AM1.5G filter (Newport 81088A), a probe stage, and a source meter with a four-wire mode (Keithley 2400), respectively. The spectrum of the solar simulator was measured by a calibrated spectroradiometer (Soma S-2440) in the wavelength range of 300 to 1350 nm. The EQE was acquired by a 300 W xenon lamp (Newport 66984) light source with a monochromator (Newprot 74112). The EQE measurement was performed by using a lock-in amplifier (Standard Research System, SR830), an optical chopper unit (SR540) operated at 260 Hz chopping frequency, and a 1Ω resistor in shunt connection to convert the photocurrent into voltage. TEM (JEOL, JEM-3000F) equipped with EELS was utilized to observe the nanoscale layer structure and composition distribution.

Ultrabroadband Pump−Probe Measurements. For ultrabroadband pump−probe measurements, a noncollinear optical parametric amplifier (NOPA) was built to produce visible laser pulses, whose spectral width is adequately broad to sustain sub-10 fs visible pulses for the measurement of ultrafast time-resolved spectroscopy. We used a regenerative chirped pulse amplifier (Legend-USP-HE; Coherent) seeded with a Ti:sapphire laser oscillator (Micra 10; Coherent: wavelength = 800 nm, pulsed width = 40 fs, repetition rate = 5 kHz) for pumping and seeding the NOPA. The beam from the regenerative amplifier was divided into two beams by using a beam splitter. One beam was utilized to generate a second harmonic of 400 nm to pump the NOPA. Another beam was focused on a sapphire plate to generate white light by inducing self-phase modulation and regarded as the seed beam of the NOPA. Finally, the NOPA generated a broad visible spectrum span over 520 to 700 nm with a nearly constant phase. A beam sampler separated the visible laser pulse into pump and probe beams. A polychromator (SP2300i; Princeton Instruments) was conducted for dispersing the probe pulse into a 128-branch fiber bundle, whose other end was split into 128 fiber branches and linked to avalanche photodiodes (APDs).

Three-Dimensional FEM Electromagnetic Simulation. Three-dimensional FEM electromagnetic simulation (COMSOL Multiphysics) was use to simulate the electromagnetic field distribution of Au NPs with 10 nm diameter embedded into CIGS device. The size of gold nanoparticles are much smaller than the incident light wavelength. We choose periodic boundary condition with 200 nm periodicity along both *x*- and *y*-directions that match the average distance of Au NPs in experimental sample. Normal incident light with linear polarization transverses to the plane of incidence (*i.e.*, TM polarization) radiated from the top of the gold nanoparticle. TM (transverse magnetic) polarized light means the electromagnetic wave in which the magnetic field vector is everywhere perpendicular to the plane of incidence (the plane of incidence is the plane spanned by the surface normal and the propagation vector of light).

Conflict of Interest: The authors declare no competing financial interest.

Supporting Information Available: Another layer structure design for plasmonic CIGS solar cells and the corresponding TEM image; angle-resolved reflectance of Au NPs in the interface of the CdS/i-ZnO layer; angle-resoled *J*−*V* characteristics; simulated electromagnetic field distribution of gap resonance; moment analysis for ultrabroadband pump−probe measurements. This material is available free of charge *via* the Internet http://pubs.acs.org/.

Acknowledgment. The research was supported by the Ministry of Science and Technology through Grant Nos. 102-2112-M-009-006-MY3, 101-2218-E-007-009-MY3, 102-2633-M-007-002, and 103-2745-M-002-004-ASP and the National Tsing Hua University through Grant No. 102N2022E1. Y.L.C. greatly appreciates the use of the facility at CNMM, National Tsing Hua University, through Grant No. 102N2744E1. Funding for this work was also provided by the Department of Industrial Technology, Ministry of Economic Affairs, Taiwan.

REFERENCES AND NOTES

1. Yang, J.; Luo, F.; Kao, T. S.; Li, X.; Ho, G. W.; Teng, J.; Luo, X.; Hong, M. Design and Fabrication of Broadband Ultralow Reflectivity Black Si Surfaces by Laser Micro/Nanoprocessing. *Light Sci. Appl.* **2014**, *3*, 185.
2. Kawakita, S.; Imaizumi, M.; Sumita, T.; Kushiya, K.; Ohshima, T.; Yamaguchi, M.; Matsuda, S.; Yoda, S.; Kamiya, T. Super Radiation Tolerance of CIGS Solar Cells Demonstrated in Space by MDS-1 Satellite. *Proc. 3rd WCPEC* **2003**, 693–696.
3. del Cueto, J. A.; Rummel, S.; Kroposki, B.; Osterwald, C.; Anderberg, A. Stability of CIS/CIGS Modules at the Outdoor Test Facility Over Two Decades. *Proc. 33th IEEE Photovoltaic Spec. Conf.* **2008**, 1–6.
4. Kim, D. I.; Park, S. W.; Park, S. R.; Baek, J. Y.; Yun, T. Y.; Han, H. J.; Jeon, C. W. Long-Term Efficiency Gain of Cu(In,Ga)Se_2 Solar Cell. *39th IEEE Photovoltaic Spec. Conf.* **2013**, 1980–1982.
5. Rockett, A.; Birkmire, R. W. $CuInSe_2$ for Photovoltaic Applications. *J. Appl. Phys.* **1991**, *70*, 81–97.
6. Green, M. A.; Emery, K.; Hishikawa, Y.; Warta, W.; Dunlop, E. D. Solar Cell Efficiency Tables (Version 44). *Prog. Photovolt: Res. Appl.* **2014**, *22*, 701–710.
7. Jackson, P.; Hariskos, D.; Lotter, E.; Paetel, S.; Wuerz, R.; Menner, R.; Wischmann, W.; Powalla, M. New World Record Efficiency for Cu(In,Ga)Se_2 Thin-Film Solar Cells Beyond 20%. *Prog. Photovoltics: Res. Appl.* **2011**, *19*, 894–897.
8. Chang, J. C.; Chuang, C. C.; Guo, J. W.; Hsu, S. C.; Hsu, H. R.; Wu, C. S.; Hsieh, T. P. An Investigation of $CuInGaSe_2$ Thin Film Solar Cells by Using CuInGa Precursor. *Nanosci. Nanotechnol. Lett.* **2011**, *3*, 200–203.

9. Chen, S. C.; Hsieh, D. H.; Jiang, H.; Liao, Y. K.; Lai, F.-I.; Chen, C. H.; Luo, C. W.; Juang, J. Y.; Chueh, Y. L.; Wu, K. H.; *et al.* Growth and Characterization of $Cu(In,Ga)Se_2$ Thin Films by Nanosecond and Femtosecond Pulsed Laser Deposition. *Nanoscale Res. Lett.* **2014**, *9*, 280.
10. Kapur, V. K.; Bansal, A.; Le, P.; Asensio, O. I. Non-Vacuum Processing of $CuIn_{1-x}Ga_xSe_2$ Solar Cells on Rigid and Flexible Substrates Using Nanoparticle Precursor Inks. *Thin Solid Films* **2003**, *431*−*432*, 53–57.
11. Calixto, M. E.; Dobson, K. D.; McCandless, B. E.; Birkmire, R. W. Controlling Growth Chemistry and Morphology of Single-Bath Electrodeposited $Cu(In,Ga)Se_2$ Thin Films for Photovoltaic Application. *J. Electrochem. Soc.* **2006**, *153*, G521–G528.
12. Wei, S. H.; Zhang, S. B.; Zunger, A. Effects of Ga Addition to $CuInSe_2$ on Its Electronic, Structural, and Defect Properties. *Appl. Phys. Lett.* **1998**, *72*, 3199–3201.
13. Liu, C. H.; Chen, C. H.; Chen, S. Y.; Yen, Y. T.; Kuo, W. C.; Liao, Y. K.; Juang, J. Y.; Lai, C. H.; Chen, L. J.; Chueh, Y. L. Large Scale Single-Crystal $Cu(In,Ga)Se_2$ Nanotip Arrays for High Efficiency Solar Cell. *Nano Lett.* **2011**, *11*, 4443–4448.
14. Igalson, M.; Zabierowski, P.; Przado, D.; Urbaniaka, A.; Edoff, M.; Shafarmanc, W. N. Understanding Defect-related Issues Limiting Efficiency of CIGS Solar Cells. *Sol. Energy Mater. Sol. Cells* **2009**, *93*, 1290–1295.
15. Ritchie, R. H. Plasma Losses by Fast Electrons in Thin Films. *Phys. Rev.* **1957**, *106*, 874–881.
16. Jain, P. K.; El-Sayed, M. A. Plasmonic Coupling in Noble Metal Nanostructures. *Chem. Phys. Lett.* **2010**, *487*, 153–164.
17. Auguie, B.; Barnes, W. L. Collective Resonances in Gold Nanoparticle Arrays. *Phys. Rev. Lett.* **2008**, *101*, 143902.
18. Jensen, T. R.; Malinsky, M. D.; Haynes, C. L.; Van Duyne, R. P. Nanosphere Lithography: Tunable Localized Surface Plasmon Resonance Spectra of Silver Nanoparticles. *J. Phys. Chem. B* **2000**, *104*, 10549–10556.
19. Chan, G. H.; Zhao, J.; Hicks, E. M.; Schatz, G. C.; Van Duyne, R. P. Plasmonic Properties of Copper Nanoparticles Fabricated by Nanosphere Lithography. *Nano Lett.* **2007**, *7*, 1947–1952.
20. Hägglund, C.; Apell, S. P. Plasmonic Near-Field Absorbers for Ultrathin Solar Cells. *J. Phys. Chem. Lett.* **2012**, *3*, 1275–1285.
21. Chen, W. T.; Wu, P. C.; Chen, C. J.; Weng, C. J.; Lee, H. C.; Yen, T. J.; Kuan, C. H.; Mansuripur, M.; Tsai, D. P. Manipulation of Multidimensional Plasmonic Spectra for Information Storage. *Appl. Phys. Lett.* **2011**, *98*, 171106.
22. Chen, W. T.; Yang, K. Y.; Wang, C. M.; Huang, Y. W.; Sun, G.; Chiang, I. D.; Liao, C. Y.; Hsu, W. L.; Lin, H. T.; Sun, S.; *et al.* High-Efficiency Broadband Meta-Hologram with Polarization-Controlled Dual Images. *Nano Lett.* **2014**, *14*, 225–230.
23. Jain, P. K.; Lee, K. S.; El-Sayed, I. H.; El-Sayed, M. A. Calculated Absorption and Scattering Properties of Gold Nanoparticles of Different Size, Shape, and Composition: Applications in Biological Imaging and Biomedicine. *J. Phys. Chem. B* **2006**, *110*, 7238–7248.
24. Pillai, S.; Catchpole, K. R.; Trupke, T.; Green, M. A. Surface Plasmon Enhanced Silicon Solar Cells. *J. Appl. Phys.* **2007**, *101*, 093105.
25. Paris, A.; Vaccari, A.; Calà Lesina, A.; Serra, E.; Calliari, L. Plasmonic Scattering by Metal Nanoparticles for Solar Cells. *Plasmonics* **2012**, *7*, 525–534.
26. Nakayama, K.; Tanabe, K.; Atwater, H. A. Plasmonic Nanoparticle Enhanced Light Absorption in GaAs Solar Cells. *Appl. Phys. Lett.* **2008**, *93*, 121904.
27. Orgassa, K.; Rau, U.; Nguyen, Q.; Schock, H. W.; Werner, J. H. Role of the CdS Buffer Layer as an Active Optical Element in $Cu(In,Ga)Se_2$Thin-Film Solar Cells. *Prog. Photovol. Res. Appl.* **2002**, *10*, 457–463.
28. Govorov, A. O.; Zhang, W.; Skeini, T.; Richardson, H.; Lee, J.; Kotov, N. A. Gold Nanoparticle Ensembles as Heaters and Actuators: Melting and Collective Plasmon Resonances. *Nanoscale Res. Lett.* **2006**, *1*, 84–90.
29. Richardson, H. H.; Hickman, Z. N.; Govorov, A. O.; Thomas, A. C.; Zhang, W.; Zhang, M. E. Thermooptical Properties of Gold Nanoparticles Embedded in Ice: Characterization of Heat Generation and Melting. *Nano Lett.* **2006**, *6*, 783–788.
30. Bohren, C. F.; Huffman, D. R. *Absorption and Scattering of Light by Small Particles*; Wiley: New York, 2008.
31. Mertz, J. Radiative Absorption, Fluorescence, and Scattering of a Classical Dipole Near a Lossless Interface: A Unified Description. *J. Opt. Soc. Am. B* **2000**, *17*, 1906–1913.
32. Atwater, H. A.; Polman, A. Plasmonics for Improved Photovoltaic Devices. *Nat. Mater.* **2010**, *9*, 205–213.
33. Zhu, J.; Hsu, C. M.; Yu, Z.; Fan, S.; Cui, Y. Nanodome Solar Cells with Efficient Light Management and Self-Cleaning. *Nano Lett.* **2010**, *10*, 1979–1984.
34. Ferry, V. E.; Munday, J. N.; Atwater, H. A. Design Considerations for Plasmonic Photovoltaics. *Adv. Mater.* **2010**, *22*, 4794–4808.
35. Sze, S. M.; Ng, K. K. *Physics of Semiconductor Devices*; John Wiley & Sons: New York, 2007.
36. Reinhard, P.; Chirila, A.; Blosch, P.; Pianezzi, F.; Nishiwaki, S.; Buecheler, S.; Tiwari, A. N. Review of Progress Toward 20% Efficiency Flexible CIGS Solar Cells and Manufacturing Issues of Solar Modules. *IEEE J. Photovolt.* **2013**, *3*, 572–580.
37. Chen, M. W.; Chau, Y. F.; Tsai, D. P. Three-Dimensional Analysis of Scattering Field Interactions and Surface Plasmon Resonance in Coupled Silver Nanospheres. *Plasmonics* **2008**, *3*, 157–164.
38. Chau, Y. F.; Chen, M. W.; Tsai, D. P. Three-dimensional Analysis of Surface Plasmon Resonance Modes on a Gold Nanorod. *Appl. Opt.* **2009**, *48*, 617–622.
39. Su, K.-H.; Wei, Q.-H.; Zhang, X.; Mock, J. J.; Smith, D. R.; Schultz, S. Interparticle Coupling Effects on Plasmon Resonances of Nanogold Particles. *Nano Lett.* **2003**, *3*, 1087–1090.
40. Chen, S. C.; Liao, Y. K.; Chen, H. J.; Chen, C. H.; Lai, C. H.; Chueh, Y. L.; Kuo, H. C.; Wu, K. H.; Juang, J. Y.; Cheng, S. J.; *et al.* Ultrafast Carrier Dynamics in $Cu(In,Ga)Se_2$ Thin Films Probed by Femtosecond Pump-Probe Spectroscopy. *Opt. Express* **2012**, *20*, 12675–12681.
41. Othonos, A. Probing Ultrafast Carrier and Phonon Dynamics in Semiconductors. *J. Appl. Phys.* **1998**, *83*, 1789–1830.
42. Wilke, R. I.; Cho, S.; Lu, H.; Schaff, W. J. Ultrafast Recombination in Si-doped InN. *Appl. Phys. Lett.* **2006**, *88*, 112111.
43. Liu, J.; Yabushita, A.; Taniguchi, S.; Chosrowjan, H.; Imamoto, Y.; Sueda, K.; Miyanaga, N.; Kobayashi, T. Ultrafast Time-Resolved Pump−Probe Spectroscopy of PYP by a Sub-8 fs Pulse Laser at 400 nm. *J. Phys. Chem. B* **2013**, *117*, 4818–4826.